applied sciences

MDPI

Article

Analysis of Sealing Characteristics of Lip Seal Rings for Deep-Sea Separable Pressure Vessels

Xuepeng Liu *, Shiping He and Jianhua Zheng

School of Mechanical Engineering, Hubei University of Technology, Wuhan 430068, China; shiping_he@sina.com (S.H.); zhengjianhua196547@163.com (J.Z.)
* Correspondence: xiaoliu19981018@163.com; Tel.: +86-13296511653

Abstract: Deep-sea pressure vessels are specialized pressure vessels designed for automatic deployment from underwater to the surface. These vessels find extensive applications in underwater life-saving and transportation. Their interiors are furnished with a pair of sealing rings, one of which is lip-shaped, and the other is a convex shape, to ensure a dependable seal. With increasing water depth, the sealing rings experience augmented pressure, resulting in a gradual pressing of the rings into the sealing groove. Using ANSYS workbench finite element software, a two-dimensional axisymmetric lip seal finite element model using forces for overall constraint was established, the complete process of progressive pressing into the sealing groove was simulated, and the deformation, contact stress, maximum shear stress, and von Mises stress distribution was also simulated. We also conducted a comparative analysis of lip seals under low and high-water pressure sealing conditions. The findings of the study indicate that when subjected to a combined effect of the installation pre-tightening force and the working water pressure, the lip seal experiences complete compression into the sealing groove at a specific water depth. When subjected to the simultaneous influence of water pressure on the sealing ring material and friction force on the contact surface, two extremes of contact stress manifest in the primary sealing zone of the lip seal. These extremes have the capacity to elevate the contact stress and the effective sealing width, ultimately leading to an improvement in the sealing performance. Concurrently, as the water pressure gradually increases, the inner concave circle of the sealing ring experiences stretching, leading to a reduction in stress concentration, equivalent stress, and shear stress to a considerable extent. This mechanism ensures that the lip-shaped sealing ring retains sufficient strength. This study offers a viable solution for conducting sealing studies on deep-sea separable pressure vessels.

Keywords: lip seal; seal performance; contact stress extremum

Citation: Liu, X.; He, S.; Zheng, J. Analysis of Sealing Characteristics of Lip Seal Rings for Deep-Sea Separable Pressure Vessels. *Appl. Sci.* **2023**, *13*, 6843. https://doi.org/10.3390/app13116843

Academic Editor: Cesare Biserni

Received: 12 May 2023
Revised: 2 June 2023
Accepted: 3 June 2023
Published: 5 June 2023

1. Introduction

A considerable proportion of pressure vessels utilized in underwater scenarios rely on an integrated design scheme to ensure the effectiveness of the sealing mechanism. The integration of fasteners, such as latches and bolts, is commonly employed to avoid leakage issues during the storage and transportation phases [1,2]. Nevertheless, the utilization of fasteners is governed by certain constraints. The research team devised a separable pressure vessel that is capable of being deployed from underwater to the surface autonomously and unfolds automatically. The vessel is anchored to the perimeter trap support using fastening straps, and its primary prototype is illustrated in Figure 1. To ensure that the separable underwater pressure vessel meets the requirements of use under various working conditions, two seals are used: a lip seal and a convex seal. The complete pressing of the two seals into the installation groove is contingent upon the installation pre-load of the fastening band, as well as the two factors of water pressure. A comprehensive analysis of the seal compression process via simulation is thus warranted. For the lip seal, water ingress into the seal cavity occurs, and the higher the water pressure, the closer the lip

seal fits the upper and lower ball housing surfaces [3]. Therefore, it represents a pivotal research focus.

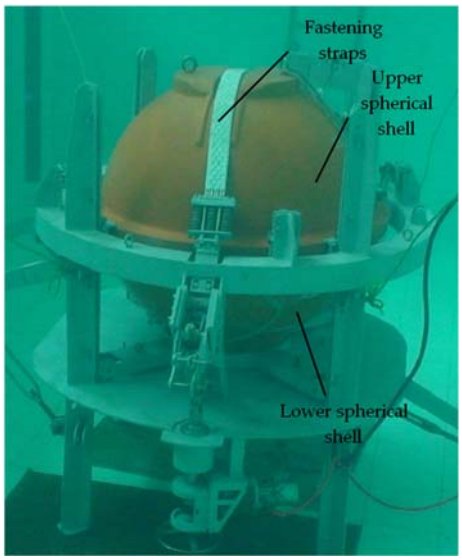

Figure 1. Principle prototype of the separable sealed pressure vessel.

Tan Feng et al. studied the effects of lip curvature, lip height, and lip thickness on sealing performance and optimized the structural parameters of the lip seal [4]. Huo Junjie et al. conducted a finite element simulation of the lip seal working in hydraulic oil, analyzed the effect of hydraulic oil temperature on the seal, and derived the changes in the sealing performance of the seal under different working temperatures [5]. Chen Guoqiang et al. established a simulation model based on the lip seal used in a high-pressure flow valve, scrutinized the impact of factors such as medium pressure and surface friction factor on the seal stress condition, and determined the stress condition of the seal boundary conditions [6]. Chen Min et al. performed a simulation-based analysis of a bespoke non-standard lip seal they had designed. They computed the deformation and stress incurred at varying initial interference and oil pressure conditions and derived the contact stress, contact width, and initial interference variation curves [7].

This study centers on investigating the performance of a lip seal implemented in a separable pressure vessel. A physical model of the lip seal is established, encompassing the pre-compression stage until the complete compression phase into the seal groove. This study aims to analyze the sealing features and performance of the lip seal throughout its entire working process. The findings of this research could offer guidance for the design of seals in comparable devices.

2. Seal Calculation Model

2.1. Seal Structure and Force Analysis

Figure 2 shows a schematic diagram of seal installation in a separable sealed pressure vessel. In accordance with the operational necessities of the separable pressure vessel, it is imperative that the upper and lower spherical shells are not rigidly interconnected by means of bolts or other permanent fastening components. The sealing structure is mainly composed of the upper spherical shell, lower spherical shell, lip seal ring, and convex seal ring, as shown in Figure 3. The specific seal dimensions are shown in Figure 4.

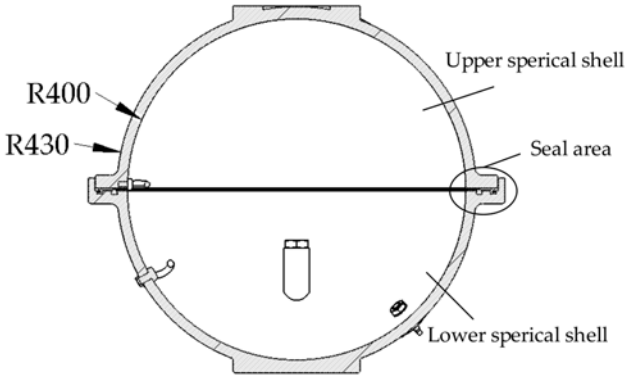

Figure 2. Seal installation position.

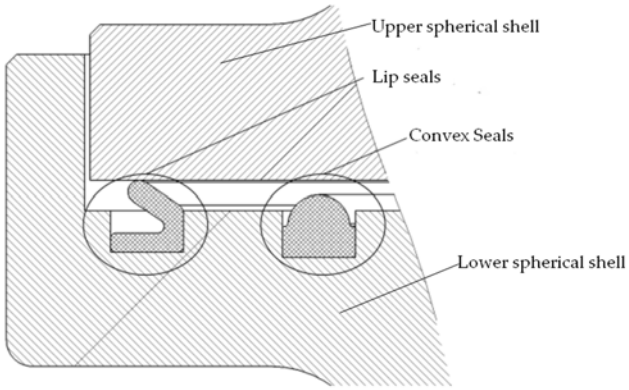

Figure 3. Lip seal sealing structure.

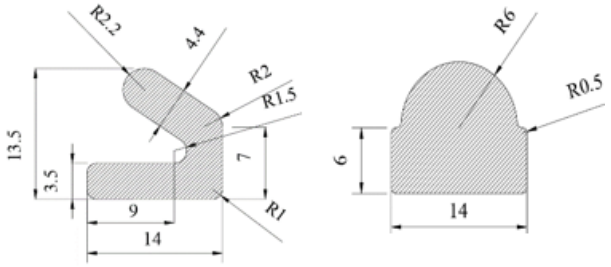

Figure 4. Seal dimensions.

After installation and pre-tightening of the fastening band, the upper and lower spherical shells of the separable pressure vessel are brought into contact, and the seal is compressed vertically, resulting in a balance between the resistance force and the compression force of the fastening band. At this point, the seal is not completely pressed into the groove. Afterward, as water pressure is applied, the upper spherical shell gradually exerts downward pressure until both the upper and lower spherical shells are tightly fitted, and the seal is vertically compressed to its limit. As a result, the seal used in the separable pressure vessel can be categorized into two conditions: the first condition pertains to shallow water with low water pressure, where the vertical compression of the seal is subject to variations based on the water depth; the second condition pertains to deep water operations, wherein the lip seal is fully compressed into the groove as the underwater vehicle descends to a certain depth. The vertical compression of the seal reaches its maximum, and the water pressure acting on the lip seal opening and inner cavity proportionally increases with the water depth.

The vertical compression force between the upper and lower spherical shells can be calculated by Equation (1).

$$F = F_{\text{preload force}} + PS \tag{1}$$

where $F_{\text{preload force}}$ denotes the initial preload force that is supplied by the fastening band, P denotes the actual water pressure exerted on the lip seal at a particular water depth, and S denotes the projected area of the spherical shell.

2.2. Material Model

The material used for both lip seals and convex seals is NBR. This material can be modeled as an incompressible hyperplastic material that exhibits complex boundary conditions and non-linearities in its mechanical properties [8]. The currently employed finite element models of rubber materials include [9–11] the Neo-Hookean strain energy function based on statistical thermodynamics, the Lord–Shulman and Green–Lindsay theories for the generalized thermoelasticity model [12] and the Mooney–Rivlin model, the Klosenr–Segal model, and the Ogden–Tschoegl model based on phenomenological theory. In this paper, we employed the two-parameter Mooney–Rivilin model and expressed the strain function as [13]:

$$\mathrm{w} = C_{10}(I_1 - 3) + C_{01}(I_2 - 3) \tag{2}$$

where w is the strain energy density function; I_1 and I_2 are the two main invariants of the strain tensor; C_{10} and C_{01} are material parameters related to the material modulus of elasticity E and material hardness H. The Equation representing the data fitting relationship is as follows [14,15]: the values of C_{10}, C_{01}, and the modulus of elasticity E are determined by calculation to be 1.46, 0.37, and 10.98 MPa, respectively.

$$\begin{cases} \lg E = 0.0198H - 0.5432 \\ E = 6(C_{10} + C_{01}) \\ C_{01} = 0.25C_{10} \end{cases} \tag{3}$$

The upper and lower spherical shells are constructed from FRP, which possesses the following physical parameters: elastic modulus E = 18.2 GPa, Poisson's ratio = 0.25, allowable stress = 241 Mpa, density = 1.8 g/cm^3. Due to the considerably higher modulus of elasticity of the upper and lower spherical shells in comparison to that of the seal material, their deformation is deemed negligible in relation to the seal.

2.3. Seal Structure and Force Analysis

A finite element method (FEM) has been used here to get the solutions to seal problems. The finite element method is a powerful numerical approach originally developed for solving nonlinear problems, and it continues to be the method of choice for complex nonlinear systems [16,17]. Because of the symmetrical shape and operational characteristics of the seal, both its structure and the loads it endures are entirely symmetrical. As a result, a two-dimensional axisymmetric model is employed for simulation calculations. The ANSYS Workbench software was utilized to develop a model of the upper and lower spherical shells of the pressure vessel along with the lip seal. Considering the seal was not subjected to any pressure, the distance between the upper and lower spherical shells was 5 mm. The mesh was divided, as illustrated in Figure 5, with a refined contact boundary. A total of 13,671 nodes and 12,675 cells were generated. The contact between the seal and the two sealing surfaces was defined as frictional contact, with a friction coefficient of 0.3 [18]. The Normal Lagrange method was employed to avert any plausible interpenetration between the seal and the sealing surfaces.

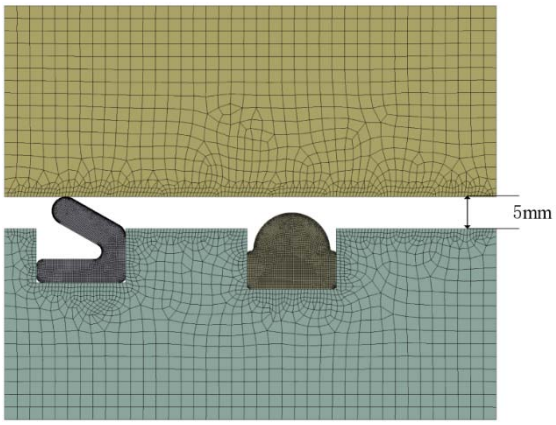

Figure 5. Finite element model of the seal.

Boundary Conditions

The finite element analysis comprises multiple load steps:

① The lower spherical shell is completely fixed, and a preloading force of 20 kN is imposed on the upper spherical shell to simulate the downward pressure exerted on it following the application of the preload force;

② Calculate the vertical compressive force on the pressure vessel at different water depths using Equation (1) and apply it to the upper spherical shell to simulate the gradual downward pressure exerted on the shell by water pressure;

③ Subject the lip seal and the inner cavity surface to a pressure load to simulate the effects of water pressure on the seal, as depicted in Figure 6.

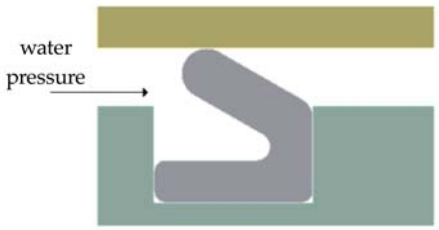

Figure 6. Water pressure path.

3. Results and Analysis

3.1. The Process of Compression and Deformation of the Seal

The forces acting on the upper spherical shell of the model at different water depths were calculated using Equation (1) and simulated in ANSYS Workbench to obtain the resulting downward displacement of the upper spherical shell at varying water depths. The obtained results are summarized in Table 1.

Table 1. Displacement of the upper spherical shell in the downward direction.

Depth (m)	Force (kN)	Downward Displacement of the Upper Spherical Shell (mm)
0	20	3.3097
1	26.998	3.5753
2	33.997	3.8074
3	40.996	3.9097
6	61.993	4.3431
10	89.989	4.6835
12	103.987	4.8618
14	117.985	5.0009

Table 1 shows that when a pre-tension force of 20 kN is applied to the fastening strap, the downward movement of the upper shell is 3.3097 mm underwater at a depth of 0 m, which represents the vertical compression of the sealing ring. At this stage, the upper and lower shells are not completely joined, and further compression of the sealing ring is still feasible. Ultimately, at a water depth of 14 m, the upper and lower shells are fully joined, and the sealing ring is entirely compressed into the groove. Subsequently, when subjected to high water pressure, the vertical compression of the sealing ring exhibits constancy and remains unchanged.

During the course of utilizing this particular seal, the state of vertical compression may experience deformation and changes. This is in stark contrast to the typical utilization of bolted connections or other such methods for firmly fastening pressure vessel seals in their operational state. It should be noted that when the water depth is relatively shallow, the level of vertical compression in the seal is decreased, necessitating the careful consideration of corresponding sealing performance requirements.

3.2. Lip Seal Strength

The finite element calculations of the deformation and stress of the seal at different water depths are shown in Figures 7 and 8.

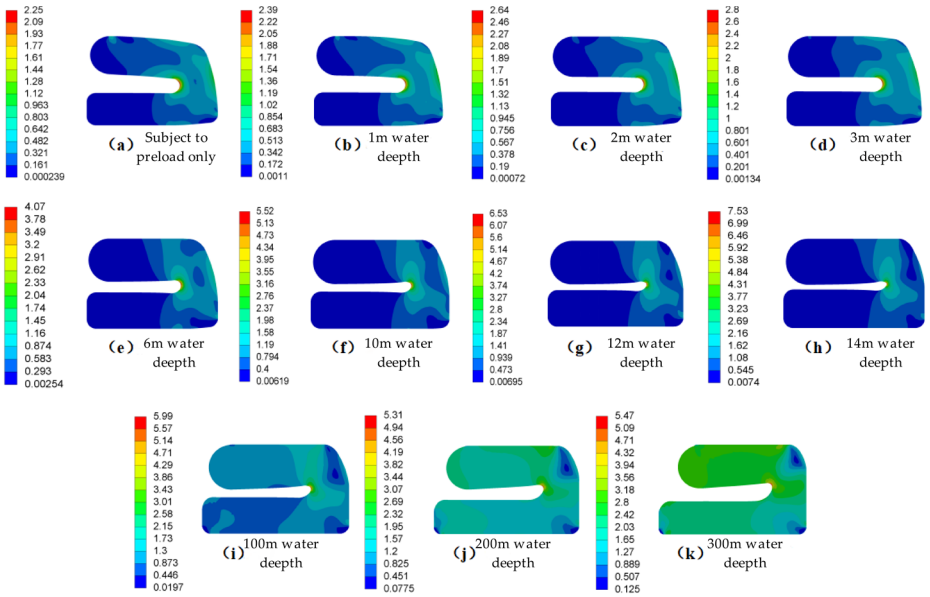

Figure 7. Stress distribution and deformation of the lip seal von Mises at different water depths.

Based on the data depicted in Figure 7a–h, it is apparent that the degree of vertical compression within the sealing ring exhibits a gradual increase as the depth of water increases from 0 to 14 m. This trend is attributed to the progressive convergence of the upper and lower lips, which move closer together. At a water depth of 14 m, the seal is fully compressed into the groove, and the internal cavity space between the upper and lower lips experiences the most severe compression. However, as the water depth continues to increase beyond 14 m, the degree of vertical compression within the seal no longer increases. Instead, the water pressure acting on the inner cavity space increases, causing it to gradually expand. This behavior is exemplified in Figure 7i–k. Based on the data presented in Figure 7, it is evident that the maximum equivalent stress and maximum shear stress occur in the bottom area of the inner lip cavity. This area represents a point of heightened susceptibility for the sealing ring with regard to potential failure mechanisms, such as tearing and fatigue.

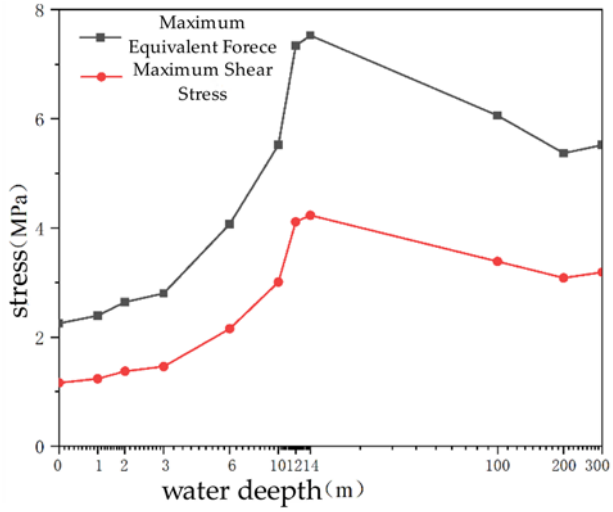

Figure 8. Maximum equivalent force and maximum shear stress on lip seal at different water depths.

According to the data presented in Figure 8, it is evident that the maximum shear stress and maximum equivalent stress of the lip seal ring both increases in proportion to the water pressure up to the point at which the upper and lower sphere shells come into full contact with each other. After the upper and lower sphere shells are fully in contact, the data presented in Figure 8 shows that the maximum equivalent stress and maximum shear stress in the lip seal ring actually decrease as water pressure continues to increase.

As depicted in Figure 9a,b, prior to the installation of the upper and lower spherical shells, an increase in water pressure resulted in noticeable vertical deformation of the lip seal. As a result, the upper and lower lips moved progressively closer together, leading to the most severe folding and squeezing of the material at the bottom of the inner cavity (i.e., the area marked by the black circle). Furthermore, the internal space was also subjected to compression. In contrast to Figures 8c and 9b, once the water depth exceeds 14 m and the upper and lower spherical shells are fitted together, the lip seal no longer exhibits increasing vertical deformation. As the depth of the water increases, the water pressure entering the inner cavity of the lip seal also increases. This increase in pressure props open the bottom of the inner cavity, thereby relieving the equivalent force and shear stress that would otherwise be present. When the lip seal of a separable sealed pressure vessel is fully fitted to the upper and lower spherical shell surfaces (i.e., the seal is fully pressed into the groove), the equivalent force and shear stress reach their maximum. As the water depth increases beyond this point, the stress decreases, which improves the sealing performance of the lip seal, reduces the risk of failure, and extends its service life.

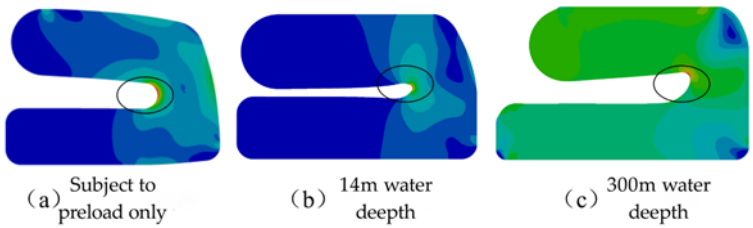

Figure 9. Comparison of internal cavity deformation of lip seals at various water depths.

3.3. Lip Seal Sealing Performance

The sealing performance of a seal depends primarily on the magnitude and distribution of the contact stress. When the contact stress exceeds the water pressure, the seal will not leak. Furthermore, when the effective contact width is greater than the width of the water pressure, the maximum contact stress will also exceed the water pressure. In other words, the greater the effective sealing pressure difference, the better the sealing

performance [19]. Figure 10 illustrates the distribution of contact stress in the primary sealing area of the lip seal at various water pressures.

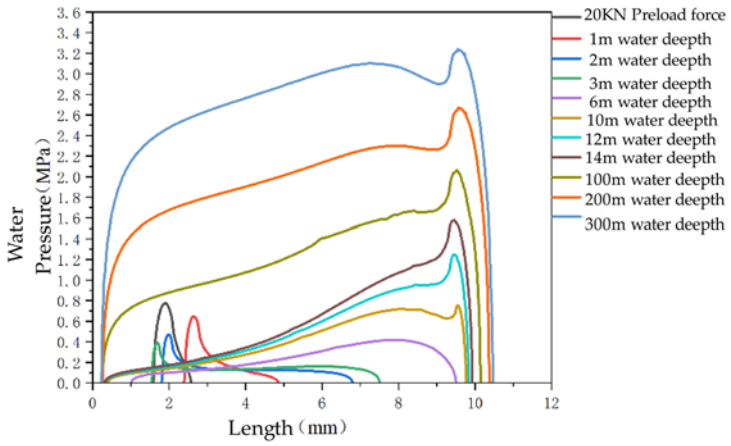

Figure 10. Distribution of contact stress in the main sealing area of the lip seal at different water depths.

As water pressure increases, the maximum contact stress of a lip seal in working conditions also increases continuously, and it always exceeds the water pressure. To analyze and assess the sealing performance of the seal, Table 2 presents the effective seal width and effective seal pressure difference of the lip seal at different water pressures. The effective seal pressure difference refers to the disparity between the maximum contact pressure and the prevailing water pressure, while the effective seal width represents the extent of the region where the contact pressure exceeds the current water pressure.

Table 2. Effective sealing width and effective sealing pressure difference for lip seals at different water depths.

Water Depth m	Effective Seal Width B/mm	Effective Seal Pressure Difference Δp/MPa
0	2.6838	0.7761
1	2.5573	0.6369
2	5.2102	0.4501
3	6.1423	0.3612
6	8.8669	0.3575
10	8.9864	0.6539
13	8.9147	1.3837
14	8.9123	1.4398
100	6.7419	1.0613
200	5.1756	0.6847
300	2.4516	0.2408

At water depths ranging from 0 to 3 m, the contact area between the lip seal and the sealing surface of the upper spherical shell increases gradually from small to large. Consequently, the peak contact stress decreases gradually, and the effective sealing pressure difference also decreases progressively. As the water depth increases, the displacement of the upper spherical shell under pressure increases. Consequently, the lip seal is gradually flattened, and its effective sealing width increases gradually, compensating for the adverse effect of the decreasing sealing pressure difference. At water depths ranging from 3 to 10 m, the seal stabilizes as the effective seal pressure differential and the effective seal width gradually increase. Beyond a water depth of 10 m, the effective seal width gradually decreases while the effective seal pressure differential increases, resulting in a complementary state. This complementary state helps to maintain the seal state stably under low water pressure. When the water depth exceeds 100 m, the effective sealing width and pressure

differential of the lip seal gradually decrease, leading to a weakening of the sealing effect under high-water pressure.

To explain the extreme points of contact stress that appear behind the main sealing area of the lip seal in Figure 10 when the water depth exceeds 10 m, it is necessary to observe the contact stresses and deformations in detail. Figure 11 compares the contact stress distribution and nodal displacement vectors of the lip seal at different water depths.

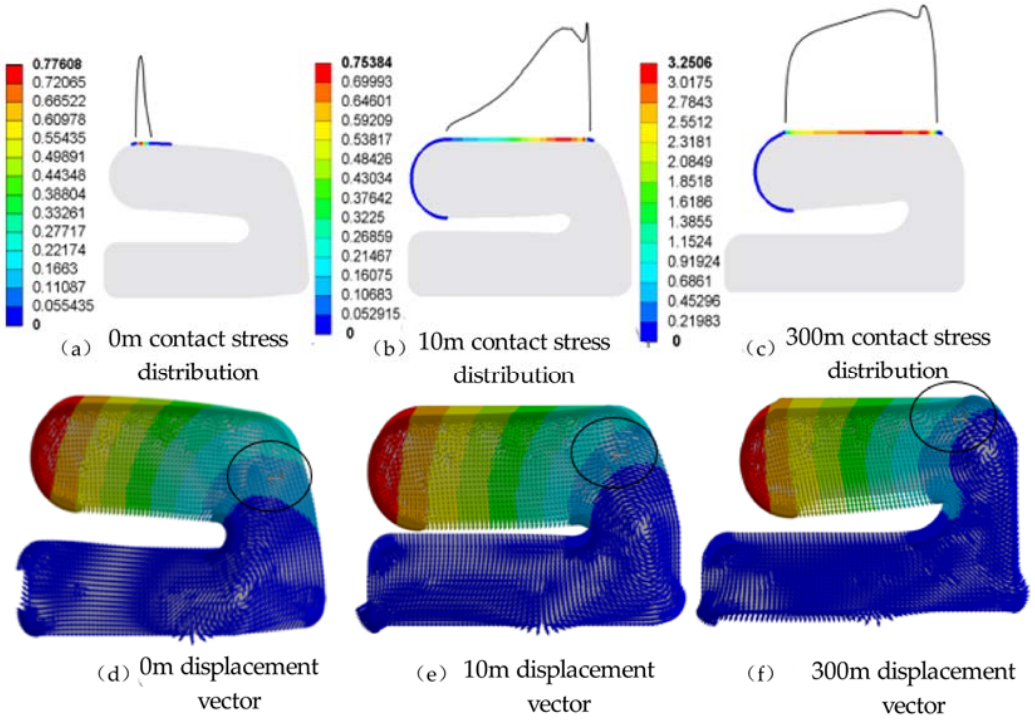

Figure 11. Comparison of the distribution of contact stress and deformation displacement vectors at various points on the lip seal at different water depths.

Figure 11a–c illustrates how the contact stress distribution changes with variations in water depth. Initially, the contact area between the lip seal and the shell surface is limited to the upper left end of the seal due to the supporting effect of the two seals. This leads to a smaller contact area and higher contact stress. As the water pressure acting on the upper spherical shell intensifies, the seal progressively compresses, leading to an expansion in the contact area and a concomitant reduction in the contact stress. As the water pressure increased, the peak contact stress shifted downstream, forming a pattern of two contact stress extreme points at a water depth of 10 m. Subsequently, as water pressure continued to increase, the peak contact stress downstream near the shoulder of the lip seal experienced a significant rise, surpassing the upstream extreme point.

Figure 11d–f depicts the displacement vector of the lip seal deformation following installation by preload only, as well as at water depths of 10 m and 300 m underwater. At a water depth of 0 m, the upper surface of the lip seal experiences downward pressure exerted by the upper cover, while the bottom surface serves as a supportive base. The behavior of the upper part of the seal resembles that of a cantilever beam undergoing bending. The displacement direction remains consistent across all nodes. Notably, the surface of the seal's shoulder, delineated by the circled area in the figure, undergoes stretching, causing the previously rounded corners to become straightened. As the water depth increases from 0 m, the downward pressure on the upper part of the seal intensifies, resulting in an amplified bending deformation. Simultaneously, the inner cavity surface of the lip seal experiences a gradual increase in water pressure. Considering that the seal is composed of an incompressible super-elastic material, the water pressure acts as a compressive force on the seal. Consequently, the deformation of the seal under water pressure conforms to the

characteristic of maintaining a constant volume [20,21]. In conjunction with the geometric constraints imposed on the remaining surfaces of the seal, the seal material inevitably shifts towards the free surface, leading to displacement variations at each node, as depicted in Figure 11e,f. Notably, the center of the displacement vortex progressively migrates towards the upper right corner, in proximity to the seal shoulder. Upon closer examination of the direction of displacement within the seal shoulder material, it becomes evident that the seal undergoes continuous compression towards the seal shoulder as the water depth increases. This compression corresponds to the occurrence of downstream contact stress extremes. Conversely, the material upstream of the seal experiences a downstream compression due to the water pressure, leading to a gradual increase in contact stress. There is friction between the main sealing area on the upper surface of the seal and the upper spherical shell surface, and the squeezing effect at both ends of the lip seal cannot be transferred to the entire main sealing line, thus forming two local contact stress peaks and raising the peak contact stress.

4. Conclusions

An underwater separable pressure vessel has been designed to integrate a lip seal and a convex seal in its sealing structure. After several years of service, this design has been installed in multiple underwater vehicles and subjected to inspection. The results indicate that the seals are functioning properly and achieving effective sealing performance, with no instances of seal failure detected.

This paper employs the ANSYS Workbench finite element simulation software to analyze the sealing process of the lip seal, from the initial state to complete compression, and to investigate the sealing groove under the influence of water pressure in both stages. Based on the simulation results, the following conclusions have been drawn:

(1) Two extremes of contact stress can be observed on the primary sealing surface of the lip seal ring analyzed in this study, resulting in an enlargement of the effective sealing width and a consequent improvement in the sealing performance. The mechanism underlying this phenomenon is attributed to two factors: the extrusion deformation of the seal ring material under the influence of water pressure and the friction occurring on the primary sealing surface;

(2) The maximum equivalent force and maximum shear stress in the lip seal are both located at the bottom of the lip cavity. As the water pressure increases prior to the complete fitting of the upper and lower spherical shells, the extrusion of the inner cavity of the lip seal intensifies, leading to an increase in both the maximum equivalent force and maximum shear stress. These values reach their peak when the upper and lower spherical shells are fully fitted. Subsequently, as the water pressure continues to rise, it alleviates the extrusion of the inner cavity of the lip seal. After this point, both the maximum equivalent force and maximum shear stress decrease with increasing water pressure, which benefits the enhancement of seal strength and prolongs its service life.

Moreover, it is imperative to conduct additional research to explore effective ways of utilizing the two contact stress extremes and enhancing the sealing performance of lip seals.

Author Contributions: Conceptualization, X.L.; writing—original draft, X.L.; writing—reviewing and editing, X.L., S.H. and J.Z.; methodology, X.L.; validation, X.L.; formal analysis, X.L.; data curation, X.L.; supervision, S.H. and J.Z. All authors have read and agreed to the published version of the manuscript.

Funding: This research received no external funding.

Institutional Review Board Statement: Not applicable.

Informed Consent Statement: Not applicable.

Data Availability Statement: All simulation data in this study are represented in the paper.

Acknowledgments: The authors thank all reviewers who helped to improve this manuscript.

Conflicts of Interest: The authors declare no conflict of interest.

References

1. Ding, J.-L. Sealing Structure Design of pack-ing box Based on Underwater Vehicles. *Mech. Res. Appl.* **2017**, *30*, 115–117.
2. Tian, Y. A Study on Determination Methods of Fasteners Preload and Thread Friction Torque in Vessel Sealing Structures. Master's Thesis, Zhejiang University of Technology, Zhejiang, China, 2008.
3. Ma, E. *Hydraulic and Pneumatic Transmission*; Higher Education Press: Beijing, China, 2010.
4. Tan, F.; Yang, B.; Huang, L.; Ding, J.; Li, Z. Study on the Structure Optimization of Shield Tunneling Machine's Main Drive Seal. *Lubr. Eng.* **2022**, *47*, 116–123.
5. Huo, J.J.; Gao, F. Medium parameters effect on sealing performance of lip seal ring. *Coal Mine Mach.* **2018**, *39*, 58–62.
6. Chen, G.Q.; Tan, J.P.; Chen, H. Failure mechanism of U-ring seal in water valve with high pressure and large flow capacity. *J. Cent. South Univ. (Sci. Technol.)* **2013**, *44*, 942–948.
7. Chen, M.; Jiang, X.; Zhao, Z.; Huang, X. The non-linearcontact finite element analysis of the mouth shaped rubber seal-ing ring. *Lubr. Eng.* **2009**, *34*, 76–79.
8. Chen, X.D. Finite Element Analysis and Optimization Design on Seal Structure of Vessel under High Pressure. Master's Thesis, Lanzhou University, Lanzhou, China, 2015.
9. Liu, D.-L.; Zhang, S.-F.; Wang, T.-L.; Cao, S.-H. Numerical analysis on the effect of hydrostatic pressure on sealing performance of O-ring of underwater glider. *J. Dalian Marit. Univ.* **2019**, *45*, 26–34. [CrossRef]
10. Rivlin, R.S.; Saunders, D.W. Large elastic deformations of isotropic materials. Strain Distribution around a hole in a sheet. *Philos. Trans. R. Soc.* **1951**, *243*, 289–298.
11. Fired, I.; Johonson, A.R. Nonliner computation of axisymmetric solid rubber deformation. *Comput. Methods Appl. Mech. Eng.* **1988**, *67*, 241–253. [CrossRef]
12. Ibrahim, A.A. Finite Element analysis of the thermoelastic interactions in an unbounded body with a cavity. *Forsch. Im Ing.* **2007**, *71*, 215–222. [CrossRef]
13. Yeoh, O.H. Characterization of elastic properties of carbon black filled rubber vulcanization. *Rubber Chem. Technol.* **1990**, *63*, 792–805. [CrossRef]
14. Fan, Z.M.; Li, L.; Wang, Q.L. Sealing performance analysis of O-ring seals in deep sea and high pressure environment. *J. Mech. Electr. Eng.* **2019**, *36*, 131–135.
15. Tao, Y.; Zhao, Y.; Yi, S.; Zhang, H.; Feng, D. Effect of MEC Seal Structure on Sealing Performance and Structural Strength. *Lubr. Eng.* **2022**, *47*, 94–100.
16. Zenkour, A.M.; Abbas, I.A. Nonlinear Transient Thermal Stress Analysis of Temperature-Dependent Hollow Cylinders Using a Finite Element Model. *Int. J. Struct. Stab. Dyn.* **2014**, *14*, 1450025. [CrossRef]
17. Saeed, T.; Abbas, I. Finite element analyses of nonlinear DPL bioheat model in spherical tissues using experimental data. *Mech. Based Des. Struct. Mach.* **2020**, *50*, 1287–1297. [CrossRef]
18. Wu, Q.; Suo, S.F.; Liu, X.F.; Huang, W.F.; Wang, Y.M. Static Sealing and Pseudo-sealing Characteristics of NITrile Rubber O-ring. *Lubr. Eng.* **2012**, *37*, 5–11.
19. Liu, Q.; Yin, Y.; Xu, H.; Chen, Z. Finite Element Analysis of Triangular Groove Sealing Performance for Large Cabin on Submersible. *Lubr. Eng.* **2021**, *46*, 163–170.
20. Qamar, S.Z.; Akhtar, M.; Pervez, T.; Al-Kharusi, M.S. Mechanical and structural behavior of a swelling elastomer under compressive loading. *Mater. Des.* **2013**, *45*, 487–496. [CrossRef]
21. Wu, K.S.; Xu, D.P.; Yan, Y.F.; Lin, F.Q.; Hu, F.T.; Kang, H. Data processing method of rubber testing based on incompressible large deformation analysis. *Rubber Ind.* **2013**, *60*, 400–403.